Metal–Organic Frameworks

DOI: 10.1002/anie.201005537

Soluble Prussian Blue Nanoworms from the Assembly of Metal–Organic Block Ionomers**

*Xavier Roy, Joseph K.-H. Hui, Muhammad Rabnawaz, Guojun Liu, and Mark J. MacLachlan**

Progress in metal–organic coordination frameworks is thriving owing to the high degree of control over their properties afforded by judicial selection of their building blocks. The thermodynamic stability of the crystalline framework for these materials has made the investigation of their bulk phase convenient and successful,[1] but this stability is now the main obstacle associated with preparing nanoscale forms of these materials. Forming discrete, nanosized metal–organic coordination frameworks is a goal that may offer the opportunity to integrate new functions into their nanoscale analogues[2] and enable incorporation of these materials into new devices.

Prussian blue (PB) is a metal–organic coordination framework of $Fe_4[Fe(CN)_6]_3{\cdot}nH_2O$ constructed from iron(II) or iron(III) vertices bridged by cyanide ligands.[3] PB and cyanometalate analogues of the general chemical formula $M'_a[M''(CN)_x]_b$ can exhibit electronic delocalization and magnetic communication between the metal centers, leading to fascinating optical, electronic, and magnetic properties.[4] Nanostructured PBs, primarily nanoparticles, have been prepared by several approaches[5] and are now being explored for applications including electrochromic materials,[6] molecule-based magnets,[7] electrocatalysts[8] and photoswitches.[7b,9]

Phase-separated block copolymers offer unique reaction environments for assembling[10] and patterning[11] organic,[12] organic–inorganic hybrid,[13] and fully inorganic[14] nanomaterials. Polymers containing an ionic block are especially remarkable because of their exceptionally low critical micelle concentration and their ability to assemble into "frozen" aggregates that could potentially be used to create and pattern nanomaterials.[12b,15] One type of ionic block copolymers, called block ionomers,[16] has been used for the preparation of quantum dots and metal nanoparticles,[17] but to our knowledge, it has never been employed in the fabrication of nanostructured metal–organic coordination frameworks.

Herein we present the synthesis and characterization of a novel comb-type metal–organic block ionomer and demonstrate its assembly into soluble worm-like PB nanostructures that can form organized two-dimensional arrays upon evaporation. The nanomaterial formed from Fe^{III}/Fe^{II} can be further calcined in air to form mesoporous iron oxide films. Interestingly, PB nanostructures are known to exhibit superparamagnetism[18] and other types of magnetic ordering.[19] We envision that our materials could find application as soluble and patternable nanomagnetic materials and as precursors for multimetallic oxide catalysts.

Our approach to construct soluble PB nanoworms is illustrated in Figure 1a. A diblock copolymer (PS-*b*-PHEMA) containing 270 styrene and 30 hydroxyethylmethacrylate (HEMA) repeat units, as measured (M_n) by size exclusion chromatography (SEC), was synthesized and found to have a narrow polydispersity index (PDI = 1.04). The PHEMA block was then functionalized with bromoacetyl bromide and further reacted with 4,4′-bipyridine to obtain pendant monoquaternized 4,4′-bipyridinium bromide substituents.

The bipyridinium-functionalized block ionomer (BI) is soluble in DMSO, DMF, halogenated solvents, THF, 1,4-dioxane, and toluene. NMR spectroscopy confirms the structure of the BI and also provides the first evidence of its assembly in solution. The ^1H NMR spectrum of the BI in $[D_6]$DMSO shows all the expected resonances as broad peaks. When the BI is dissolved in a less-polar solvent, such as $[D_8]$THF, it assembles into reverse micelles with the ionic block in the rigid core. These large aggregates have no dynamic equilibrium between micelles and single chains on the NMR timescale as confirmed by the absence of the ionic block signals in the NMR spectrum.

Metal complexation of the block ionomer was accomplished by slowly adding an aqueous solution of $Na_3[Fe(CN)_5NH_3]$ and [18]crown-6 to a THF solution of BI. We used UV/Vis spectroscopy to monitor the change in the electronic structure of the polymer at each step of the synthesis. After dilution and filtration, the resulting comb-type pentacyanoferrate(II) block ionomer $[Fe^{II}(CN)_5]$BI is blue in THF (4% v/v H_2O) as a consequence of a metal-to-ligand charge transfer (MLCT) transition centered at around 685 nm (Figure 1b, trace B) and analogous to that measured for the model compound ([18]crown-6)sodium (*N*-methyl-4,4′-bipyridinium)pentacyanoferrate(II) (Figure 1b, trace A). We monitored the complexation reaction by UV/Vis spectroscopy and observed no further increase in the intensity of the MLCT band after 90 min for our typical experimental

[*] X. Roy, J. K.-H. Hui, Prof. M. J. MacLachlan
Department of Chemistry, University of British Columbia
2036 Main Mall, Vancouver, BC, V6T 1Z1 (Canada)
Fax: (+1) 604-822-2847
E-mail: mmaclach@chem.ubc.ca
M. Rabnawaz, Prof. G. Liu
Department of Chemistry, Queen's University
90 Bader Lane, Chernoff Hall, Room 411
Kingston, ON, K7L 3N6 (Canada)

[**] We thank the Natural Sciences and Engineering Research Council of Canada and UBC for funding. X.R. thanks the FQRNT and NSERC for postgraduate scholarships. We also thank the UBC Bioimaging Facility for assistance.

Supporting information for this article is available on the WWW under http://dx.doi.org/10.1002/anie.201005537.

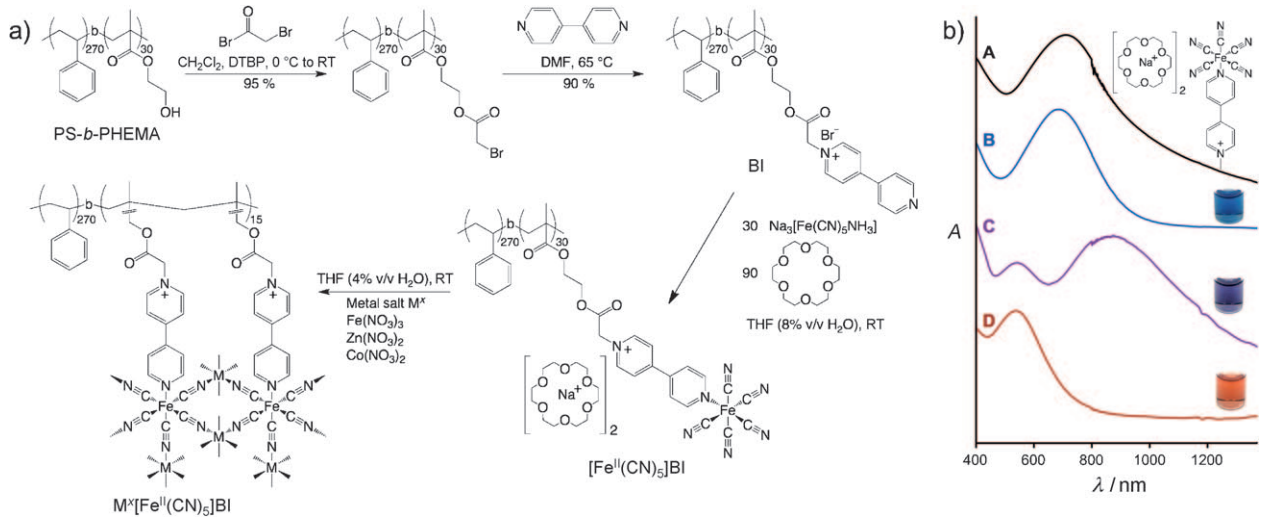

Figure 1. a) Synthesis of the metal–organic block ionomer $[Fe^{II}(CN)_5]BI$ and its crosslinking into the PB framework $M^x[Fe^{II}(CN)_5]BI$ (DTBP = 2,6-di-*tert*-butylpyridine). b) UV/Vis spectra in THF (with 4% v/v H_2O) of A) the model compound ([18]crown-6)sodium (*N*-methyl-4,4′-bipyridinium)-pentacyanoferrate(II) (shown), B) $[Fe^{II}(CN)_5]BI$, C) $Fe^{III}[Fe^{II}(CN)_5]BI$, and D) $Zn^{II}[Fe^{II}(CN)_5]BI$. Photographs of the respective solutions are also included in (B)–(D) as a visual reference for the color change.

complexation conditions (1 mg mL^{-1} $[Fe^{II}(CN)_5]BI$ in THF with 8% v/v H_2O). We anticipated $[Fe^{II}(CN)_5]BI$ to aggregate in solution because of its amphiphilic nature and, as expected, only the PS block is observed in the NMR spectrum of $[Fe^{II}(CN)_5]BI$.

The metal-containing polymer $[Fe^{II}(CN)_5]BI$ can be reacted with different transition metal salts such as $Fe(NO_3)_3$, $Zn(NO_3)_2$ and $Co(NO_3)_2$ to crosslink the $\{Fe(CN)_5\}$ terminal groups into PB-type frameworks. We label our materials with the general formula $M^x[Fe^{II}(CN)_5]BI$, where M represents the crosslinking metal with oxidation state $x+$. In all cases, the resulting product is soluble in THF (4% v/v H_2O) and ^{1}H NMR data was obtained for the diamagnetic species $Zn^{II}[Fe^{II}(CN)_5]BI$. As with the unlinked polymer, $[Fe^{II}(CN)_5]BI$, only the PS block is observed. The mixed-valence compound $Fe^{III}[Fe^{II}(CN)_5]BI$ is purple and exhibits a broad transition centered around 875 nm (Figure 1b, trace C) that we assign to intervalence charge transfer (IVCT) between the cyanide-bridged iron centers, akin to that known for bulk PB.[20] The MLCT band, which is still present, is blue-shifted by 140 nm (relative to $[Fe^{II}(CN)_5]BI$) to around 545 nm and confirms that the $\{Fe^{II}(CN)_5\}$ complex is still coordinated to the block ionomer. $Zn^{II}[Fe^{II}(CN)_5]BI$, which is not expected to have any valence delocalization as Zn^{II} has a d^{10} electronic configuration, shows the same blue-shift for the MLCT, but no IVCT band (Figure 1b, trace D). These data support the conversion of the BI-tethered metal complexes into an extended PB-type metal–organic coordination framework.

Further evidence for the connectivity of the PB network was obtained by IR spectroscopy of the solid materials purified by precipitation in water. IR spectra of the different polymeric materials consistently show peaks attributable to both organic blocks and to the pentacyanoferrate(II) complex. Of particular interest is the energy of the ν_{CN} stretching band, which is diagnostic of the coordination environment for the iron cyanide complex. The approximately C_{4v}-symmetric precursor complex $Na_3[Fe(CN)_5NH_3]$ exhibits three ν_{CN} stretching modes, with the strongest band at 2030 cm^{-1}. Exchanging the amine group with the strong π-accepting bipyridinium ligand upon metalation of BI results in a 20 cm^{-1} blue-shift for the ν_{CN} stretching mode of $[Fe^{II}(CN)_5]BI$ to 2050 cm^{-1}. Crosslinking $[Fe^{II}(CN)_5]BI$ into the various M^x-$[Fe^{II}(CN)_5]BI$ causes this ν_{CN} stretching band to shift to even higher energies (2060–2085 cm^{-1}). This blue-shift is a well-established trend for cyanide ligands on going from a terminal to a bridging mode as expected for the formation of PB-type frameworks.[21]

Energy-dispersive X-ray analysis (EDX) and thermogravimetric analysis (TGA) confirmed the incorporation of iron and the other metal in the polymeric materials. Atomic ratios (M^x/Fe) ranging from 1.2 to 1.6 are typically measured with no alkali metal observed. TGA of $[Fe^{II}(CN)_5]BI$ showed a 95% weight loss between 100 and 500 °C, which is ascribed to the thermal decomposition and removal of the organic portion of the polymer. For $M^x[Fe^{II}(CN)_5]BI$, 88 to 90 wt% is typically lost by calcination under N_2, as measured by TGA.

We used transmission electron microscopy (TEM) to investigate the assembly of the metal–organic block ionomers dropcast from THF with 4% v/v H_2O solutions onto TEM grids. The worm-like nanostructures observed for $[Fe^{II}(CN)_5]BI$ and $Fe^{III}[Fe^{II}(CN)_5]BI$ are shown in Figure 2a,b. TEM images of these two materials are similar, although $Fe^{III}[Fe^{II}(CN)_5]BI$ had significantly better contrast than $[Fe^{II}(CN)_5]BI$, which also exhibited some degradation under the electron beam. These observations are consistent with the $Fe^{III}[Fe^{II}(CN)_5]BI$ nanoworms being made of metal-crosslinked PB cores, as crosslinking is well-known to improve the stability of polymers under the electron beam.[22] The inner diameter of the cylindrical micelles is monodisperse throughout the materials and reproducible for all of the polymeric compounds. High magnification micros-

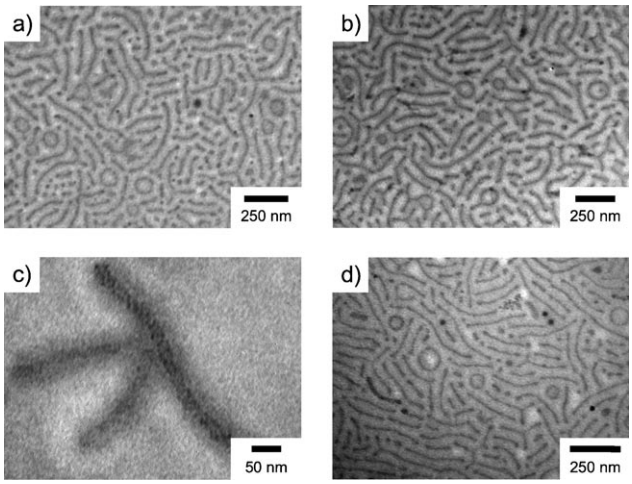

Figure 2. Transmisssion electron microscopy (TEM) characterization of the polymeric materials dropcast on TEM grids. a,b) Images of $[Fe^{II}(CN)_5]$BI (a) and $Fe^{III}[Fe^{II}(CN)_5]$BI (b). c) A high-magnification image of a single $Fe^{III}[Fe^{II}(CN)_5]$BI nanoworm; d) the nanoscale structure obtained with $Zn^{II}[Fe^{II}(CN)_5]$BI.

copy shows a (19.9 ± 1.4) nm diameter PB core and a (24.1 ± 3.1) nm thick PS corona for isolated $Fe^{III}[Fe^{II}(CN)_5]$BI worms (Figure 2c). Beam-induced sample degradation prevented comparable high magnification images of $[Fe^{II}(CN)_5]$BI from being acquired. Similar nanostructures were obtained for the mixed-metal PB analogues (Figure 2d) for $Zn^{II}[Fe^{II}(CN)_5]$BI, as well as for materials that were allowed to stand in solution for 24 h before dropcasting on a TEM grid. The UV/Vis and IR spectra were also unaffected by the aging process. We observed a small proportion of toroidal aggregates and spherical micelles in all of the samples, regardless which linking metal was used. This result suggests that the shape of the aggregates is not controlled by the coordination geometry of the linking metal. We are currently working at selectively producing these diversely shaped aggregates.

We hypothesized that the metal-containing block ionomer $[Fe^{II}(CN)_5]$BI self-assembles into nanoworms in THF with the iron cyanide complex ionic block in the core. Addition of transition metals then crosslinks the iron cyanide core into a PB-type framework and slow evaporation organizes these nanoworms into a tightly packed structure, which can also be described as a thin PS film with ordered embedded monodisperse PB nanowires. The idealized supramolecular assembly and the schematic cross-sectional view of a micelle are shown in Figure 3a and b, respectively. We used dynamic light-scattering (DLS) experiments to investigate the aggregation of the polymers in solution. We measured apparent hydrodynamic radii ($R_{h,app}$) of (51.1 ± 1.2) nm and (71.0 ± 1.6) nm for BI and $[Fe^{II}(CN)_5]$BI (0.5 mg mL^{-1} in THF with 4% v/v H_2O), respectively. Our DLS data confirm that aggregation of the polymers occurs in solution, but because of the worm-like shape of the micelles, it does not provide accurate dimensions. Therefore, we used freeze-drying experiments to corroborate the DLS results and verify the existence of the nanoworms in solution. Samples of $[Fe^{II}(CN)_5]$BI and $Fe^{III}[Fe^{II}(CN)_5]$BI in 1,4-dioxane (4% v/v H_2O) deposited on TEM grids were rapidly frozen in liquid nitrogen to immobilize their solution assemblies. We verified that the same nanoworm structures are obtained by evaporation self-assembly when we replaced THF with the higher-melting 1,4-dioxane. The structures obtained after removal of the solvent by freeze-drying for $[Fe^{II}(CN)_5]$BI and $Fe^{III}[Fe^{II}(CN)_5]$BI are shown in Figure 3c and d, respectively. Disordered or isolated cylindrical micelles were observed for both polymeric materials, confirming that the nanoworms are present in solution.

In the course of our investigation, we discovered that the use of $Na_3[Fe(CN)_5NH_3]$ is not necessary to obtain the PB nanoworm assemblies. Adding an excess of $K_4[Fe(CN)_6]$ and [18]crown-6 (1:4 molar ratio) in water to a THF solution of BI (0.5 mg mL^{-1}; ca. 0.4 mM of bipyridinium groups), sonicating the resulting suspension for 1 h, and filtering the excess salt gives the block ionomer–ferrocyanide hybrid $[Fe^{II}(CN)_6]$BI as a clear THF (4% v/v H_2O) solution. $[Fe^{II}(CN)_6]$BI can then be crosslinked into a PB framework with an excess of $Fe(NO_3)_3$, and after centrifugation and filtration to remove any trace of insoluble bulk PB, soluble $Fe^{III}[Fe^{II}(CN)_6]$BI materials are obtained. UV/Vis and IR spectroscopy and EDX all confirm the formation of PB, and TGA suggests a slightly higher metal content for $Fe^{III}[Fe^{II}(CN)_6]$BI (85.5 wt% loss upon calcination) compared with $Fe^{III}[Fe^{II}(CN)_5]$BI. Once again, assemblies made of monodisperse 20 nm PB nanoworms are obtained by dropcasting $Fe^{III}[Fe^{II}(CN)_6]$BI on a TEM grid (Figure 4a). This approach is not limited to $Fe^{III}[Fe^{II}(CN)_6]$, but can be extended to different PB analogues known to have a wide range of properties and potential applications. $Co^{II}[Fe^{III}(CN)_6]$BI and $Cu^{II}[Co^{III}(CN)_6]$BI (Figure 4b) were selected as representative examples.

To test whether the bipyridinium block ionomer is necessary to generate the PB nanoworms, we synthesized a triethylammonium-functionalized block ionomer analogue (BI*; Figure 4c) and used it in our approach. Microscopy of the unfiltered $Fe^{III}[Fe^{II}(CN)_6]$BI* dropcast on a TEM grid (Figure 4d) shows that in this case, the core of the nanoworms does not contain PB, which is instead observed as crystals outside of the micelles. From this result, we infer that a coordinating ligand is necessary to anchor the PB inside the ionic core. In the approach beginning with $[M^x(CN)_6]$BI where the complex is not coordinated to the polymer, the crosslinking metal added becomes coordinated to the BI.

Interestingly, $Fe^{III}[Fe^{II}(CN)_6]$BI can be used as a precursor to iron oxide nanostructures. Calcining $Fe^{III}[Fe^{II}(CN)_6]$BI deposited on a Si/Si_3N_4 TEM grid at 450 °C for 1 h in air converted the PB nanoworm assembly into a mesoporous Fe_2O_3 film made of circa 10 nm nanofibers (Figure 4e,f). The PB nanoworms aggregated during the high-temperature oxidation to form an Fe_2O_3 nanofiber mesh. TGA confirmed complete removal of the organic template under our conditions and we indexed the PXRD pattern of the resulting material as a mixture of α-Fe_2O_3 (hematite) and γ-Fe_2O_3 (maghemite), the latter oxide being ferrimagnetic and superparamagnetic on the nanoscale. This approach could potentially be used to prepare a wide range of magnetically and catalytically active multimetallic oxide nanomaterials.

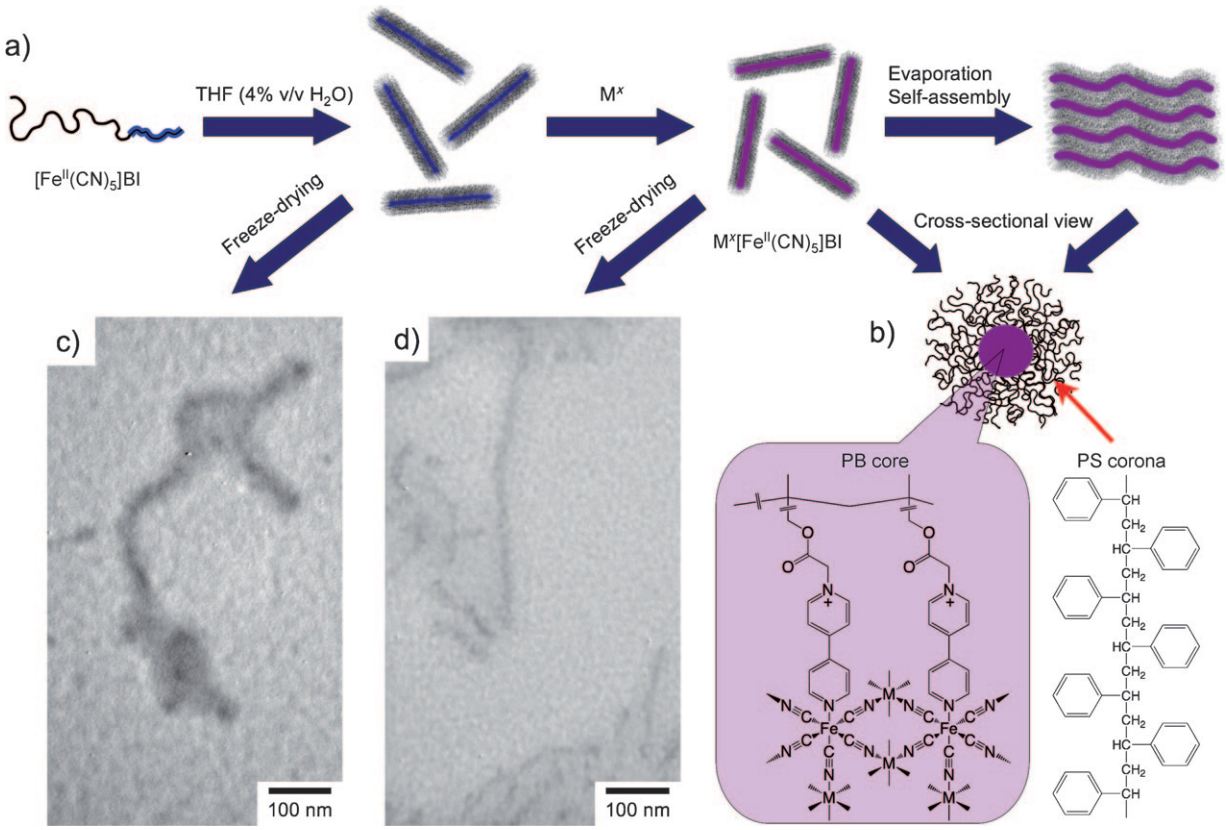

Figure 3. a) The block ionomer (BI)-mediated self-assembly of Prussian blue (PB) nanoworms. b) A cross-sectional view of a typical $M^x[Fe^{II}(CN)_5]BI$ nanoworm. As a control experiment, $[Fe^{II}(CN)_5]BI$ and $M^x[Fe^{II}(CN)_5]BI$ solutions in 1,4-dioxane (4% v/v H_2O), were rapidly frozen in liquid nitrogen and freeze-dried at −10°C (T_m for 1,4-dioxane is 11.8°C). c,d) TEM images of the c) $[Fe^{II}(CN)_5]BI$ and d) $M^x[Fe^{II}(CN)_5]BI$ freeze-dried structures.

In summary, we report the first examples of soluble PB nanoworms. A new block ionomer self-assembles in organic solvents into stable cylindrical micelles with ionic cores that can be metalated with an iron(II) cyanide complex or used as an ion confinement region for different cyanometalate compounds to be crosslinked into metal–organic frameworks. The nanoworms containing PB-type metal–organic coordination frameworks are stable in solution for hours, organize upon evaporation on surfaces, and can be used as precursors for metal oxide nanostructures. Based on the size and diversity of the PB family and the different aggregate morphologies known for block ionomers, we envision that this approach will provide a useful route to soluble and patternable nanomaterials with tunable magnetic, optical, and electronic properties.

Experimental Section

Synthesis of BI: A solution of PS-*b*-PHEMA (see Supporting Information; 300 mg) and 2,6 di-*tert*-butylpyridine (235 mg, 1.2 mmol, 5 equiv based on the HEMA unit) in dry dichloromethane (60 mL) was placed under an N_2 atmosphere and cooled to 0°C in an ice bath. Bromoacetyl bromide (250 mg, 1.2 mmol, 5 equiv based on the HEMA unit) was added dropwise to the stirring solution. The reaction mixture was warmed to room temperature and stirred for 4 h. The polymer solution was concentrated by rotary evaporation and a white powder was precipitated with acetonitrile, centrifuged, washed with acetonitrile three times, then dried under vacuum at 60°C. Yield: 312 mg (95%). The bromoacetylated block copolymer (300 mg) was dissolved in DMF (5 mL) and added dropwise to a solution of 4,4′-bipyridine (385 mg, 2.5 mmol, 10 equiv based on the HEMA unit) in DMF (5 mL). The solution was stirred at 65°C under N_2 for 18 h and the block ionomer (BI) was precipitated with acetone, centrifuged, and washed sequentially with acetone and acetonitrile (three times each). Yield: 305 mg (91%). ^{1}H NMR spectroscopy (Supporting Information, Figure S4) showed 100% conversion of the bromoacetyl groups to the bipyridinium bromide.

$[Fe^{II}(CN)_5]BI$: A solution of $Na_3[Fe(CN)_5NH_3]\cdot 3H_2O$ (17 mg, 51 μmol) and [18]crown-6 (41 mg, 155 μmol) in deionized water (4.8 mL) was added dropwise to a vigorously stirred solution of BI (60 mg) in THF (60 mL). The solution was stirred for 90 min at room temperature, then diluted with THF (60 mL), and finally filtered to afford a clear blue solution. $[Fe^{II}(CN)_5]BI$ can be precipitated in water, centrifuged and washed with water to isolate the solid material, or the solution can be used directly in the next step.

$M^x[Fe^{II}(CN)_5]BI$: $Fe(NO_3)_3\cdot 6H_2O$ (21 mg, 52 μmol) dissolved in a minimum of THF (ca. 1 mL) was added dropwise to the $[Fe^{II}(CN)_5]BI$ solution (125 mL). The $Fe^{III}[Fe^{II}(CN)_5]BI$ solution was stirred at room temperature for 30 min, then centrifuged at 4500 rpm and filtered to remove any trace of insoluble bulk Prussian blue (PB). M^x-$[Fe^{II}(CN)_5]BI$ can be precipitated in water, centrifuged, washed with water and dried under vacuum at 50°C for 24 h to isolate the solid materials (yield: 70 mg), or the solution can be dropcast to generate PB nanoworm surface assemblies. The procedure was repeated with $Zn(NO_3)_2\cdot 6H_2O$ and $Co(NO_3)_2\cdot 6H_2O$ to form Zn^{II}-$[Fe^{II}(CN)_5]BI$ and $Co^{II}[Fe^{II}(CN)_5]BI$, respectively.

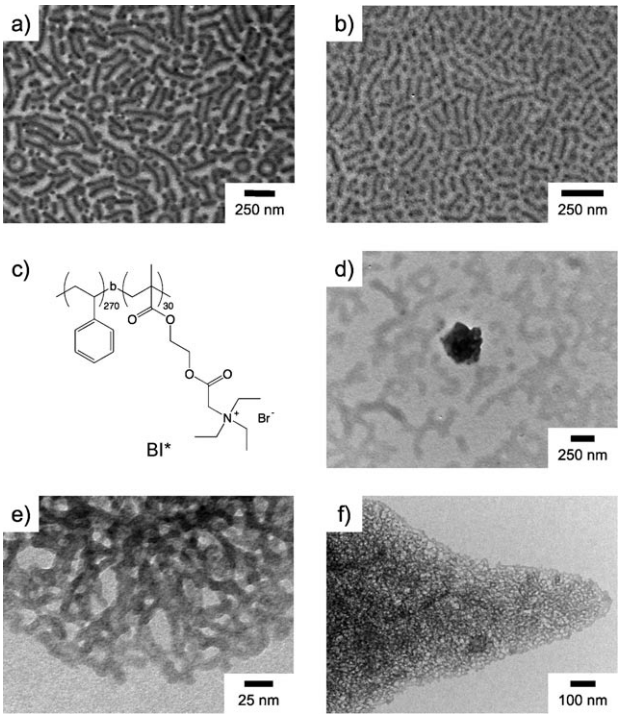

Figure 4. a,b) TEM images of a) $Fe^{III}[Fe^{II}(CN)_6]$BI and b) Cu^{II}-$[Co^{III}(CN)_6]$BI. c) The chemical structure of the triethylammonium ion functionalized block ionomer BI*. d) A TEM image when BI* is used instead of BI in the synthesis of PB nanoworms; a PB nanocrystal is seen surrounded by PB-free BI* nanoworms. e,f) High- and low-magnification TEM images of a mesoporous Fe_2O_3 film obtained by calcination of $Fe^{III}[Fe^{II}(CN)_6]$BI.

Received: September 4, 2010
Revised: November 3, 2010
Published online: January 5, 2011

Keywords: block copolymers · inorganic polymers · iron oxide · nanostructures · Prussian blue

[1] a) B. Wang, A. P. Côté, H. Furukawa, M. O'keefe, O. M. Yaghi, *Nature* **2008**, *453*, 207–211; b) S. Kitagawa, R. Kitaura, S.-i. Noro, *Angew. Chem.* **2004**, *116*, 2388–2430; *Angew. Chem. Int. Ed.* **2004**, *43*, 2334–2375; c) O. M. Yaghi, M. O'Keeffe, N. W. Ockwig, H. K. Chae, M. Eddaoudi, J. Kim, *Nature* **2003**, *423*, 705–714; d) S. R. Batten, R. Robson, *Angew. Chem.* **1998**, *110*, 1558–1595; *Angew. Chem. Int. Ed.* **1998**, *37*, 1460–1494.

[2] a) D. Tanaka, A. Henke, K. Albrecht, M. Moeller, K. Nakagawa, S. Kitagawa, J. Groll, *Nat. Chem.* **2010**, *2*, 410–416; b) X. Roy, M. J. MacLachlan, *Chem. Eur. J.* **2009**, *15*, 6552–6559; c) T. Tsuruoka, S. Furukawa, Y. Takashima, K. Yoshida, S. Isoda, S. Kitagawa, *Angew. Chem.* **2009**, *121*, 4833–4837; *Angew. Chem. Int. Ed.* **2009**, *48*, 4739–4743; d) W. J. Rieter, K. M. Pott, K. M. L. Taylor, W. Lin, *J. Am. Chem. Soc.* **2008**, *130*, 11584–11585; e) M. Oh, C. A. Mirkin, *Nature* **2005**, *438*, 651–654.

[3] a) H. J. Buser, D. Schwarzenbach, W. Petter, A. Ludi, *Inorg. Chem.* **1977**, *16*, 2704–2710; b) K. R. Dunbar, R. A. Heintz, *Prog. Inorg. Chem.* **1997**, *45*, 283–391; c) M. P. Shores, L. G. Beauvais, J. R. Long, *J. Am. Chem. Soc.* **1999**, *121*, 775–779.

[4] a) O. Sato, T. Iyoda, A. Fujishima, K. Hashimoto, *Science* **1996**, *272*, 704–705; b) S. Ferlay, T. Mallah, R. Ouahes, P. Veillet, M. Verdaguer, *Nature* **1995**, *378*, 701–703; c) K. Itaya, I. Uchida, V. D. Neff, *Acc. Chem. Res.* **1986**, *19*, 162–168; d) S. S. Kaye, J. R. Long, *J. Am. Chem. Soc.* **2005**, *127*, 6506–6507.

[5] a) X. Roy, L. K. Thompson, N. Coombs, M. J. MacLachlan, *Angew. Chem.* **2008**, *120*, 521–524; *Angew. Chem. Int. Ed.* **2008**, *47*, 511–514; b) S. Vaucher, M. Li, S. Mann, *Angew. Chem.* **2000**, *112*, 1863–1866; *Angew. Chem. Int. Ed.* **2000**, *39*, 1793–1796; c) T. Uemura, S. Kitagawa, *J. Am. Chem. Soc.* **2003**, *125*, 7814–7815; d) P. Zhou, D. Xue, H. Luo, X. Chen, *Nano Lett.* **2002**, *2*, 845–847; e) G. Liang, J. Xu, X. Wang, *J. Am. Chem. Soc.* **2009**, *131*, 5378–5379; f) R. McHale, N. Ghasdian, Y. Liu, H. Wang, Y. Miao, X. Wang, *Macromol. Rapid Commun.* **2010**, *31*, 856–860.

[6] a) D. M. DeLongchamp, P. T. Hammond, *Adv. Funct. Mater.* **2004**, *14*, 224–232; b) W. Caseri, *J. Mater. Chem.* **2010**, *20*, 5582–5592.

[7] a) S. Vaucher, J. Fielden, M. Li, E. Dujardin, S. Mann, *Nano Lett.* **2002**, *2*, 225–229; b) L. Catala, F. Volatron, D. Brinzei, T. Mallah, *Inorg. Chem.* **2009**, *48*, 3360–3370.

[8] a) A. A. Karyakin, E. A. Puganova, I. A. Budashov, I. N. Kurochkin, E. E. Karyakina, V. A. Levchenko, V. N. Matveyenko, S. D Varfolomeyev, *Anal. Chem.* **2004**, *76*, 474–478; b) E. Jin, X. Lu, L. Cui, D. Chao, C. Wang, *Electrochim. Acta* **2010**, *55*, 7230–7234; c) Z. Chu, Y. Zhang, X. Dong, W. Jin, N. Xu, B. Tieke, *J. Mater. Chem.* **2010**, *20*, 7815–7820.

[9] M. Taguchi, K. Yamada, K. Suzuki, O. Sato, Y. Einaga, *Chem. Mater.* **2005**, *17*, 4554–4559.

[10] S. Förster, M. Antonietti, *Adv. Mater.* **1998**, *10*, 195–217.

[11] a) Z. Nie, E. Kumacheva, *Nat. Mater.* **2008**, *7*, 277–290; b) C. Tang, E. M. Lennon, G. H. Fredrickson, E. J. Kramer, C. J. Hawker, *Science* **2008**, *322*, 429–432.

[12] a) D. J. Pochan, Z. Chen, H. Cui, K. Hales, K. Qi, K. L. Wooley, *Science* **2004**, *306*, 94–97; b) L. Zhang, A. Eisenberg, *Science* **1995**, *268*, 1728–1731; c) S. A. Jenekhe, X L. Chen, *Science* **1999**, *283*, 372–375.

[13] a) Y. Lin, A. Böker, J. He, K. Sill, H. Xiang, C. Abetz, X. Li, J. Wang, T. Emrick, S. Long, Q. Wang, A. Balazs, T. P. Russell, *Nature* **2005**, *434*, 55–59; b) X. Wang, G. Guerin, H. Wang, Y. Wang, I. Manners, M. A. Winnik, *Science* **2007**, *317*, 644–647; c) J. Massey, K. N. Power, I. Manners, M. A. Winnik, *J. Am. Chem. Soc.* **1998**, *120*, 9533–9540; d) C. Park, J. E. McAlvin, C. L. Fraser, E. L. Thomas, *Chem. Mater.* **2002**, *14*, 1225–1230; e) Y. Yan, N. A. M. Besseling, A. de Keizer, M. Drechsler, R. Fokkink, M. A. C. Stuart, *J. Phys. Chem. B* **2007**, *111*, 11662–11669.

[14] a) D. Zhao, J. Feng, Q. Huo, N. Melosh, G. H. Fredrickson, B. F. Chmelka, G. D. Stucky, *Science* **1998**, *279*, 548–552; b) S. C. Warren, L. C. Messina, L. S. Slaughter, M. Kamperman, Q. Zhou, S. M. Gruner, F. J. DiSalvo, U. Wiesner, *Science* **2008**, *320*, 1748–1752.

[15] a) M. Moffitt, K. Khougaz, A. Eisenberg, *Acc. Chem. Res.* **1996**, *29*, 95–102; b) D. E. Discher, A. Eisenberg, *Science* **2002**, *297*, 967–973; c) Y. Kang, J. J. Walish, T. Gorishnyy, E. L. Thomas, *Nat. Mater.* **2007**, *6*, 957–960.

[16] Ionic block copolymers in solution can be classified as either block polyelectrolytes or block ionomers, depending on the nature of the solvent. When dissolved in water, ionic block copolymers are block polyelectrolytes. They form micelles with nonionic cores and coronas made up of the soluble ionic segments. In organic solvents, ionic block copolymers are called block ionomers and they assemble into reverse micelles with ionic cores surrounded by the nonionic soluble blocks. See Ref. [15a] for more details.

[17] M. Moffitt, L. McMahon, V. Pessel, A. Eisenberg, *Chem. Mater.* **1995**, *7*, 1185–1192.

[18] a) L. Catala, T. Gacoin, J.-P. Boilot, É. Rivière, C. Paulsen, E. Lhotel, T. Mallah, *Adv. Mater.* **2003**, *15*, 826–829; b) J. G. Moore, E. J. Lochner, C. Ramsey, N. S. Dalal, A. E. Stiegman,

Angew. Chem. **2003**, *115*, 2847 – 2849; *Angew. Chem. Int. Ed.* **2003**, *42*, 2741 – 2743.
[19] a) M. Arai, M. Miyake, M. Yamada, *J. Phys. Chem. C* **2008**, *112*, 1953 – 1962; b) A. Ghirri, A. Candini, M. Evangelisti, G. C. Gazzadi, F. Volatron, B. Fleury, L. Catala, C. David, T. Mallah, M. Affronte, *Small* **2008**, *4*, 2240 – 2246.
[20] M. B. Robin, *Inorg. Chem.* **1962**, *1*, 337 – 342.
[21] S. F. A. Kettle, E. Diana, E. Boccaleri, P. L. Stanghellini, *Inorg. Chem.* **2007**, *46*, 2409 – 2416.
[22] a) J. S. Trent, J. I. Scheinbeim, P. R. Couchman, *Macromolecules* **1983**, *16*, 589 – 598; b) D. M. Huong, M. Drechsler, H.-J. Cantow, M. Möller, *Macromolecules* **1993**, *26*, 864 – 866; c) G. H. Michler, *Electron Microscopy of Polymers*, Springer, Berlin, **2008**, p. 177.

